Discrete Symmetrical Coupled Inductor Structure and its Matrix-type Implementation for DC-DC Converter

Xiang Zhang*, Shangzhi Pan†, Praveen Jain†
Queen's University, Kingston, ON, Canada
xiang.zhang@queensu.ca

***Abstract*—This paper proposed a symmetrical discrete coupling array (DCIArray) structure for multiphase interleaved DC-DC converter. Firstly, a magnetics modeling based on reluctance and mutual-inductance is discussed with analysis on both equivalent time-interval inductance and small signal dynamic model. Then, matrix-type coupling implementation of the coupled structure is investigated. Simulation based on Finite Element Software and experiments on a four-phase buck converter has verified the effectiveness of proposed structure.**

***Index Terms*—Symmetrical coupled inductors, interleaved, multiphase buck converter, matrix inductor**

I. Introduction

Multiphase symmetrical coupled inductors has a wide application in interleaved DC/DC PWM convertion system, from stepodown converters like voltage rugulators modules (VRMs) in point-of-load (PoL) applications [1], [2], [3], [4], [5], [6], [7], [8], [9], to bidirectional step-up converter like on board chargers (OBCs) [10], [11], [12].

In Buck converters, researchers have already revealed that inversely-coupled (or negative coupled) inductors could produce a higher bandwidth in transient-state, while reducing the ripple current in the steady-state [13], [2]; however, these examples only ustilize two-phase coupled structure, which prevent the multi-phase coupled inductors to fulfilling their potential in high current applications. On the other hand, even though some studies successfully extend symmetrical coupled inductors to higher phases [1], [5], [4], the magnetics components related in the coupling is always customly manufatured with special geometrical design for perticular uses, which is hard to access for industrical application. Same problems also arise in multiphase interleaved PFC or bidirectional boost or buck-boost converters, where a positive-coupled inductors are prefered to reduce the switching frequency in critical conduction mode operations [10], [14], [15].

Fig.1. (a) has summarized the modern multiphase symmetrical coupled inductor structures. Multi-leg magnetics based coupled inductors like ladder-shape and matrix coupled inductor are well investigated with both reluctance model and their inductance-dual model. However, such structure has natural negative coupling structure and the coupling coefficient is not adjustable once the core is designed, typically the coupling coefficient is fixed to a value less than $-1/m$ in the m phase system, and the coupling coefficient in either two phases is identical, ignoring the different phase position mutual inductance influence on the coupling behavior. Another research decomposed the integrated core into a special indirect coupled manner, resulting an adjustable coupling coefficient with improved transient performance but introduce extra winding and external inductor [4].

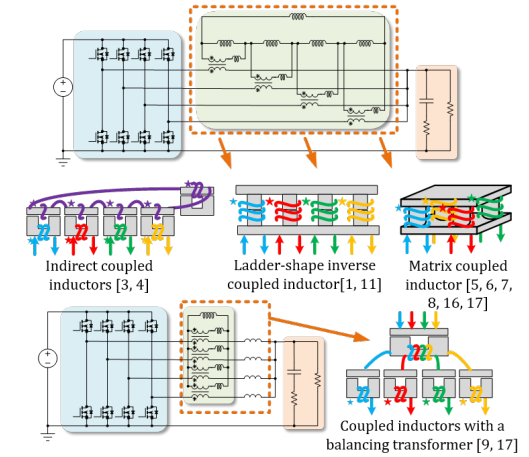

(a) Modern multiphase coupled inductor structures

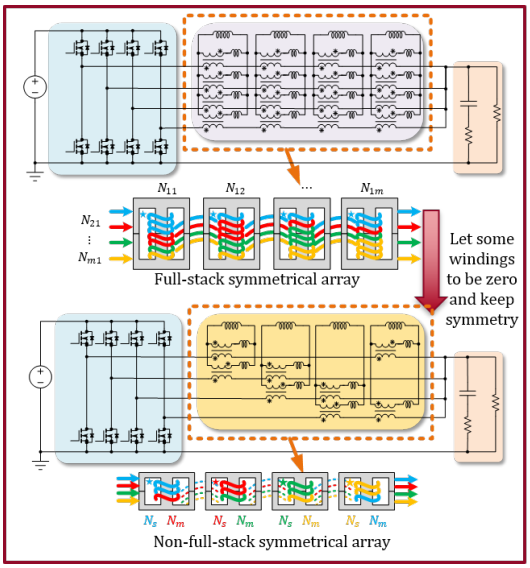

(b) Proposed discrete coupled inductor array (DCIArray)

Fig. 1. Different types of symmetrical coupled inductors structure

To tackle the abovementioned problems, this paper proposed a more flexible coupling inductance design, naming discrete coupled inductor array (DCIArray), as shown in Fig.1. (b). By simply letting some windings in each discrete coupled inductor to be direct-, inverse-, or non-coupled, the mutual

inductance between phases can be either positive or negative, or zero, so the coupling coefficient can be easily controlled. Besides, the paper also analysis the impact of phase position on coupling behavior, which always happens in non-full stack DCIArray cases. with detailed time-base equivalent inductance and small signal dynamics model. Finally, the matrix-type implementation of inductor geometrical arrangements, coil routing guidance and Finite Element simulation comparison are also displayed in the article.

II. Magnetics modeling and buck converter application example

A. Magnetics model of discrete coupled inductor array

In DCIArray, each inductor can be treated as an independent multi-winding transformer, if the leakage flux is negligent, the main flux ϕ_k for the inductor can be calculated as (1), $\mathcal{R}_k$ is the reluctance on the main flux path, supposing there are m phases in total, then

$$\phi_k = \frac{\sum_{i=1}^{m} (N_{ik} \cdot i_i)}{\mathcal{R}_k} \tag{1}$$

For every phase, the corresponding phase windings on each discrete inductor are connected in series, so the total equivalent voltage across the DCIArray can be summed up as

$$\begin{aligned} v_{Lk} &= \frac{d\left(\sum_{j=1}^{m} (N_{kj} \cdot \phi_j)\right)}{dt} \\ &= M_{1k}\frac{di_1}{dt} + \cdots + L_{sk}\frac{di_k}{dt} + \cdots + M_{mk}\frac{di_m}{dt} \end{aligned} \tag{2}$$

Then the inductance-matrix for the proposed DCIArray can be obtained. In four-phase system, when each phase is only coupled with adjacent phases as Fig.1 non-full-stack example, the mutual-inductance-matrix model $\mathbf{L}_{4\times4}$ can be expressed in (3), N_s and N_m are the self-turn and mutual turn on each inductor, assuming $\alpha = L_m/L_s$ is the coupling coefficient.

$$\begin{bmatrix} v_{L1} \\ v_{L2} \\ v_{L3} \\ v_{L4} \end{bmatrix} = \begin{bmatrix} \left(N_s^2 + N_m^2\right)/\mathcal{R}_k & (N_s N_m)/\mathcal{R}_k & 0 & (N_s N_m)/\mathcal{R}_k \\ (N_s N_m)/\mathcal{R}_k & \left(N_s^2 + N_m^2\right)/\mathcal{R}_k & (N_s N_m)/\mathcal{R}_k & 0 \\ 0 & (N_s N_m)/\mathcal{R}_k & \left(N_s^2 + N_m^2\right)/\mathcal{R}_k & (N_s N_m)/\mathcal{R}_k \\ (N_S N_m)/\mathcal{R}_k & 0 & (N_s N_m)/\mathcal{R}_k & \left(N_s^2 + N_m^2\right)/\mathcal{R}_k \end{bmatrix} \begin{bmatrix} di_1/dt \\ di_2/dt \\ di_3/dt \\ di_4/dt \end{bmatrix} = \underbrace{\begin{bmatrix} L_s & L_m & 0 & L_m \\ L_m & L_s & L_m & 0 \\ 0 & L_m & L_s & L_m \\ L_m & 0 & L_m & L_s \end{bmatrix}}_{\mathbf{L}_{4\times4}} \begin{bmatrix} di_1/dt \\ di_2/dt \\ di_3/dt \\ di_4/dt \end{bmatrix} \tag{3}$$

$$\begin{bmatrix} di_1/dt \\ di_2/dt \\ di_3/dt \\ di_4/dt \end{bmatrix} = \begin{bmatrix} L_s & L_m & 0 & L_m \\ L_m & L_s & L_m & 0 \\ 0 & L_m & L_s & L_m \\ L_m & 0 & L_m & L_s \end{bmatrix}^{-1} \begin{bmatrix} v_{L1} \\ v_{L2} \\ v_{L3} \\ v_{L4} \end{bmatrix} = \frac{1}{L_s} \begin{bmatrix} \frac{2\alpha^2-1}{4\alpha^2-1} & \frac{\alpha}{4\alpha^2-1} & \frac{-2\alpha^2}{4\alpha^2-1} & \frac{\alpha}{4\alpha^2-1} \\ \frac{\alpha}{4\alpha^2-1} & \frac{2\alpha^2-1}{4\alpha^2-1} & \frac{\alpha}{4\alpha^2-1} & \frac{-2\alpha^2}{4\alpha^2-1} \\ \frac{-2\alpha^2}{4\alpha^2-1} & \frac{\alpha}{4\alpha^2-1} & \frac{2\alpha^2-1}{4\alpha^2-1} & \frac{\alpha}{4\alpha^2-1} \\ \frac{\alpha}{4\alpha^2-1} & \frac{-2\alpha^2}{4\alpha^2-1} & \frac{\alpha}{4\alpha^2-1} & \frac{2\alpha^2-1}{4\alpha^2-1} \end{bmatrix} \begin{bmatrix} v_{L1} \\ v_{L2} \\ v_{L3} \\ v_{L4} \end{bmatrix} = \underbrace{\begin{bmatrix} B_s & B_1 & B_2 & B_1 \\ B_1 & B_s & B_1 & B_2 \\ B_2 & B_1 & B_s & B_1 \\ B_1 & B_2 & B_1 & B_s \end{bmatrix}}_{\mathcal{R}_{4\times4}} \begin{bmatrix} v_{L1} \\ v_{L2} \\ v_{L3} \\ v_{L4} \end{bmatrix} \tag{4}$$

This inductance matrix can be transformed to the reluctance matrix $\mathcal{R}_{4\times4}$ in (4) by calculating the inverse of the matrix. To find the phase current behavior, the reluctance matrix is helpful to deduce the closed-form expression, since the value of phase inductor voltage v_{Lk} can only be $v_{in} - v_o$ or $-v_o$ in every time interval.

The main difference of non-full stack DCIArray coupling from traditional multi-leg coupling structure is the non-diagonal element (mutual element) in the inductance matrix is not strictly identical [5], [16], but, still keeps a symmetrical form when look through from an individual phase. This characteristics make the current ripple in each phase perform differently in each time interval with different equivalent inductance, resulting more complex dynamics in the converter. This will be discussed in detailed in the next section.

The reluctance matrix also shows that even though some phases don't have coupling in flux linkage, they will still affect each other on their phase current. An illustration in four-phase buck converter is that the non-adjacent phases' mutual inductances are zero, but the first-derivative of their inductor current are controlled by all four phases.

B. Time interval analysis based on derived model

Based on the derived magnetic model, the current waveforms in DCIArray buck converter with corresponding gate signals under different duty cycle can be plotted in Fig.2. For four-phase system, there will be eight different time intervals in a every switching period, for case of $0 < D < 0.25$ and $0.25 < D < 0.5$, the ripple phase current will be different depending the duty cycle is overlap or not, but the current waveform will be mirror symmetrical on $D = 0.5$.

In order to present the coupling effect in each individual phase, equivalent interval inductance are utilized to describe the slope of current under different switching signal inputs. By combining the reluctance matrix in (4), we can follow the calculation process in [13], [2], then in the case of $0 < D < 0.25$ during time interval I, the current slope in the first channel can be written as (5),

$$\begin{aligned} \frac{di_1}{dt} =& \frac{1}{L_s}\frac{2\alpha^2-1}{4\alpha^2-1}(V_{in} - V_o) + \frac{1}{L_s}\left[\frac{\alpha}{4\alpha^2-1} + \right. \\ & \left. \frac{-2\alpha^2}{4\alpha^2-1} + \frac{\alpha}{4\alpha^2-1}\right] * (-V_o) = \frac{1}{L_{eq1}}(V_{in} - V_o) \end{aligned} \tag{5}$$

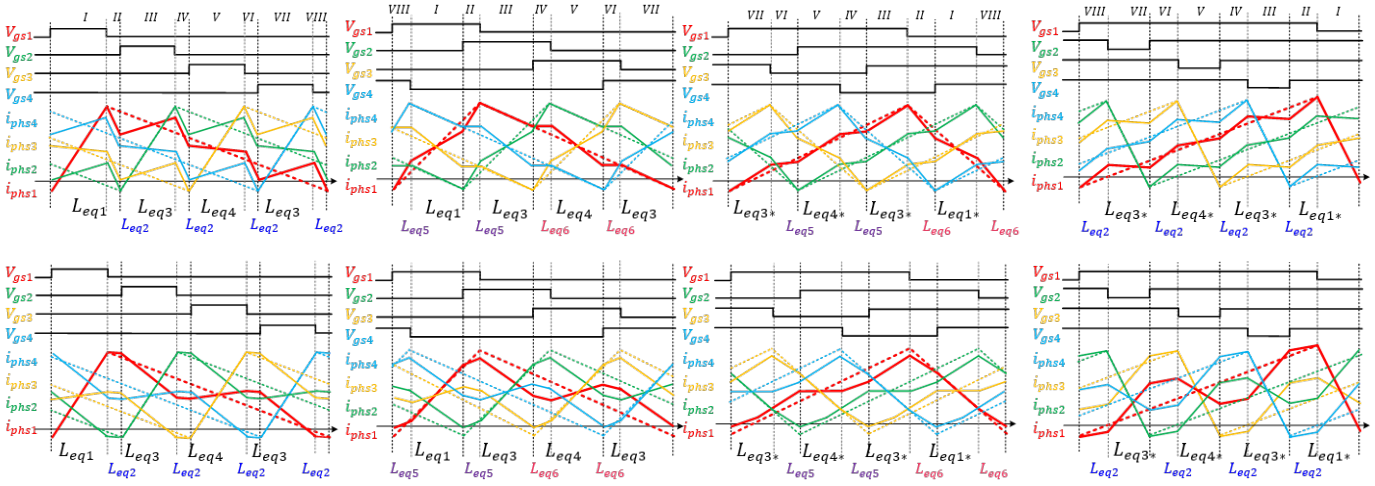

(a) $0 < D < 0.25$ (b) $0.25 < D < 0.5$ (c) $0.5 < D < 0.75$ (d) $0.75 < D < 1$

Fig. 2. Steady State phase current under different duty cycle, with equivalent inductance based on phase A (up, negative coupled; down, positive coupled)

Then the equivalent inductance in this particular time interval can be interpreted as a function of duty cycle and coupling coefficient. Similarly, during time interval II, IV, VI, and VIII, the current slope in the first channel will be (6)

$$\frac{di_1}{dt} = \frac{1}{L_s}\left[\frac{2\alpha^2-1}{4\alpha^2-1} + \frac{\alpha}{4\alpha^2-1} + \frac{-2\alpha^2}{4\alpha^2-1} + \frac{\alpha}{4\alpha^2-1}\right] * (-V_o) = \frac{1}{L_{eq2}}(-V_o) \tag{6}$$

Noting that all equivalent interval inductance is defined assuming the phase current is generated under the excitation of single channel voltage, thus the voltage on them are depending on this corresponding channel. In first channel only during interval I the voltage is $v_{in} - v_o$, the others are $-v_o$. Also duty cycle follow the balancing equation in the whole period.

$$D = v_o / v_{in} \tag{7}$$

By the above rules, all equivalent interval inductances based on the first channel can be calculated as the following table.

TABLE I
EXPRESSION OF EQUIVALENT INTERVAL INDUCTANCE IN ALL DUTY CYCLE RANGES

Duty cycle range	Related time interval	Symbol	Expression
$0 < D < 0.25$	Interval I	L_{eq1}	$\frac{(1-D)(4\alpha^2-1)}{2\alpha^2-2D\alpha+(D-1)}L_s$
	Interval II, IV, VI, VIII	L_{eq2}	$\frac{(4\alpha^2-1)}{2\alpha-1}L_s$
	Interval III, VII	L_{eq3}	$\frac{(-D)(4\alpha^2-1)}{(1-2D)\alpha+D}L_s$
	Interval V	L_{eq4}	$\frac{(-D)(4\alpha^2-1)}{-2\alpha^2-2D\alpha+D}L_s$
$0.75 < D < 1$	Interval I	L_{eq1*}	$\frac{(-D)(4\alpha^2-1)}{-2\alpha^2+(2-2D)\alpha+D}L_s$
	Interval III, VII	L_{eq3*}	$\frac{(1-D)(4\alpha^2-1)}{(1-2D)\alpha+(D-1)}L_s$
	Interval V	L_{eq4*}	$\frac{(1-D)(4\alpha^2-1)}{\alpha^2+(2-2D)\alpha+(D-1)}L_s$
$0.25 < D < 0.5$	Interval I, III	L_{eq5}	$\frac{(1-D)(4\alpha^2-1)}{2\alpha^2+(1-2D)\alpha+(D-1)}L_s$
$0.5 < D < 0.75$	Interval V, VII	L_{eq6}	$\frac{D(4\alpha^2-1)}{2\alpha^2+(2D-1)\alpha-D}L_s$

The waveform in Fig.2(a) and (b) shows that when gate signals are overlap, the equivalent inductance L_{eq2} in $0 < D < 0.25$ will break into two equivalent inductance L_{eq5} and L_{eq6} in $0.25 < D < 0.5$, also because of the current symmetry of $D = 0.5$, L_{eq1}, L_{eq3}, L_{eq4} will have a group of perfect complementary equivalent inductances as L_{eq1*}, L_{eq3*}, L_{eq4*}. So there will be nine different equivalent interval inductance in total for all duty cycle range.

C. The relation of equivalent inductance, common /differential mode inductance and steady-state /transient inductance

Modern PoL converters require larger steady-state inductance to smooth the ripple current for load devices, but also desire converter to have better dynamic regulation as lower transient inductance. So L_{ss} and L_{tr} is proposed as a pair of important parameters to evaluate the performance of coupling improvement.

L_{ss} dominates the amplitude of the steady-sate current ripple and L_{tr} affects the dynamic responds of the converter. Fig.3 has depicted the related current as i_{ripple} and Δi, respectively.

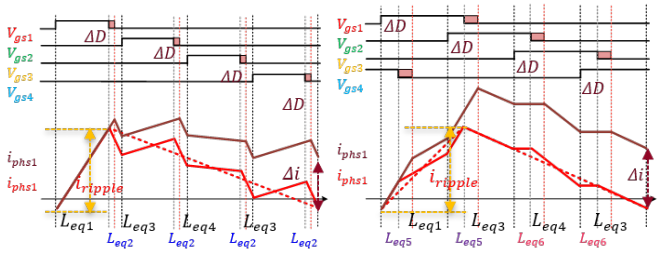

(a) $0 < D < 0.25$ (b) $0.25 < D < 0.5$

Fig. 3. Transient phase current with negative coupling

Evidently, when $0 < D < 0.25$, the steady-state inductance L_{ss} is equal to the equivalent interval inductance L_{eq1}; while in $0.25 < D < 0.5$, L_{ss} is related to both L_{eq1} and L_{eq5}. Therefore, by adding three intervals current change in Fig.3.(b) we have the equation of

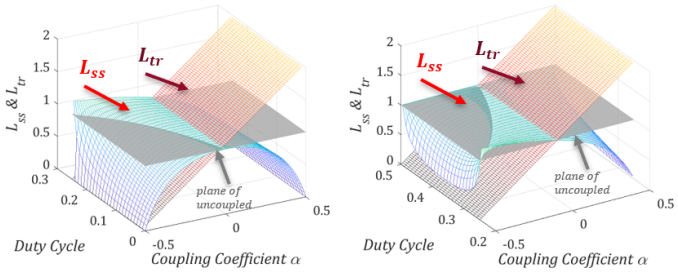

(a) $0 < D < 0.25$ (b) $0.25 < D < 0.5$

Fig. 4. Normalized L_{ss} and L_{tr} under different duty cycle and coupling coefficient

$$i_{\text{ripple}} = \frac{v_{in}-v_o}{L_{ss}}DT_s = \frac{v_{in}-v_o}{L_{eq5}}(D-0.25)T_s + \frac{v_{in}-v_o}{L_{eq1}}(0.5-D)T_s + \frac{v_{in}-v_o}{L_{eq5}}(D-0.25)T_s \tag{8}$$

After substituting (8) by the L_{eq1} and L_{eq5} in the table I, we can have the full expression of steady-state inductance when D is below 0.5.

$$L_{ss} = \begin{cases} \frac{(1-D)\left(4\alpha^2-1\right)}{2\alpha^2-2D\alpha+(D-1)}L_s & (\text{ in } 0 < D < 0.25) \\ \frac{(D-1)\left(4\alpha^2-1\right)}{2\alpha^2-\left(2D-2+\frac{1}{2D}\right)\alpha+D-1}L_s & (\text{ in } 0.25 < D < 0.5) \end{cases} \tag{9}$$

For transient inductance, it is more complicated to calculate as the current increase in one switching period comes from four intervals, as shown in (10). Considering of the inductor currents are balanced in each switching cycle there exist (11)

$$\Delta i = \left(\frac{v_{in}-v_o}{L_{eq1}} - \frac{-v_o}{L_{eq2}}\right)\Delta DT_s + \left(\frac{-v_o}{L_{eq3}} - \frac{-v_o}{L_{eq2}}\right)\Delta DT_s + \left(\frac{-v_o}{L_{eq4}} - \frac{-v_o}{L_{eq2}}\right)\Delta DT_s + \left(\frac{-v_o}{L_{eq3}} - \frac{-v_o}{L_{eq2}}\right)\Delta DT_s \tag{10}$$

$$\frac{v_{in}-v_o}{L_{eq1}}DT_s + \frac{-v_o}{L_{eq2}}(0.25-D)T_s + \frac{-v_o}{L_{eq3}}DT_s + \frac{-v_o}{L_{eq2}}(0.25-D)T_s + \frac{-v_o}{L_{eq4}}DT_s + \frac{-v_o}{L_{eq2}}(0.25-D)T_s + \frac{-v_o}{L_{eq3}}DT_s + \frac{-v_o}{L_{eq2}}(0.25-D)T_s = 0 \tag{11}$$

Similarly, when $0.25 < D < 0.5$, we can also write the current increase and balancing equation as (12) and (13)

$$\Delta i = \left(\frac{v_{in}-v_o}{L_{eq5}} - \frac{v_{in}-v_o}{L_{eq1}}\right)\Delta DT_s + \left(\frac{v_{in}-v_o}{L_{eq5}} - \frac{-v_o}{L_{eq3}}\right)\Delta DT_s + \left(\frac{-v_o}{L_{eq6}} - \frac{-v_o}{L_{eq4}}\right)\Delta DT_s + \left(\frac{-v_o}{L_{eq6}} - \frac{-v_o}{L_{eq3}}\right)\Delta DT_s \tag{12}$$

$$\frac{v_{in}-v_o}{L_{eq5}}(D-0.25)T_s + \frac{v_{in}-v_o}{L_{eq1}}(0.5-D)T_s + \frac{v_{in}-v_o}{L_{eq5}}(D-0.25)T_s + \frac{-v_o}{L_{eq3}}(0.5-D)T_s + \frac{-v_o}{L_{eq6}}(D-0.25)T_s + \frac{-v_o}{L_{eq4}}(0.5-D)T_s + \frac{-v_o}{L_{eq6}}(D-0.25)T_s + \frac{-v_o}{L_{eq3}}(0.5-D)T_s = 0 \tag{13}$$

After combining (12), (13) and (12), (13) with equation simplification, respectively, we can obtain an identical equation describing the value of transient responds of the system, written as

$$\frac{\Delta i}{\Delta D} = \frac{V_{in}}{L_{eq2}}T_s = \frac{V_{in}}{L_{tr}}T_s \tag{14}$$

(14) suggests that the transient inductance L_{tr} only related with the coupling structure of the magnetic components regardless of the steady-state duty cycle D and poarity of ΔD, as mentioned previously in [13].

Generally, as long as the symmetry is maintained in the coupling inductor, the responds of same perturbation of duty cycle applies into the inductor array will be same as zero-input responds of the array. This matches the case in time intervals of II, IV, VI, VIII when $0 < D < 0.25$ and $0.75 < D < 1$, where equivalent interval inductance are L_{eq2}. Therefore, we can conclude that in symmetrical coupled inductors, the value of transient inductance L_{tr} is a constant characteristic of a particular magnetic component, and it equals to the equivalent interval inductance L_{eq2}, also represents the common mode inductance of the magnetics components L_{CM}.

The normalized L_{ss} and L_{tr} are shown in Fig. 4 under different duty cycles and coupling coefficients; when compared to an uncoupled inductor, the green region demonstrates that negative coupling can produce both a larger L_{ss} and a smaller L_{tr} simultaneously. Furthermore, the steady-state inductance is continuous on the margin of $D = 0.25$, and L_{ss} have higher dependability to guarantee a higher value than non-coupled case as the duty cycle approaches $D = 0.25$.

D. Dynamics analysis for the multiphase discrete coupled buck converter

State space based small signal model is commonly used for the dynamic analysis in DC/DC PWM conversion system, because they provide a easy way to determine the system's transfer function as well as a good guidance for the controller design.

Firstly, we assume the buck converter has four identical winding resistances R_{wind} in every phase, a output capacitor C with equivalent series resistances of R_{esr}, a load resister R_{load} , and a symmetrical coupled inductor.

Now we can choose the state space vecter to be $\mathbf{x} = [\hat{i_1}, \hat{i_2}, \hat{i_3}, \hat{i_4}, \hat{v_c}]^T$, and output space vector as $\mathbf{y} = [\hat{i_1}, \hat{i_2}, \hat{i_3}, \hat{i_4}, \hat{v_o}]^T$. Taking each phases' duty cycle as input variables, then $\mathbf{u} = [\hat{d_1}, \hat{d_2}, \hat{d_3}, \hat{d_4}]^T$. After state averaging, the voltage across each inductor can be written as

$$v_{\hat{Lk}} = \hat{d_k}V_{in} - \hat{i_k}R_{\text{wind}} - \hat{v_o} \tag{15}$$

By substituting (15) to the the first row in the matrix of (4), we have

$$\begin{aligned} d\hat{i_1}/dt &= B_s v_{\hat{L}1} + B_1 v_{\hat{L}2} + B_2 v_{\hat{L}3} + B_1 v_{\hat{L}4} \\ &= B_s\left(\hat{d_1}V_{\text{in}} - \hat{i_1}R_{\text{wind}} - \hat{v_o}\right) + B_1\left(\hat{d_2}V_{\text{in}} - \hat{i_2}R_{\text{wind}} - \hat{v_o}\right) \\ &+ B_2\left(\hat{d_3}V_{\text{in}} - \hat{i_3}R_{\text{wind}} - \hat{v_o}\right) + B_1\left(\hat{d_4}V_{\text{in}} - \hat{i_4}R_{\text{wind}} - \hat{v_o}\right) \end{aligned} \tag{16}$$

$$\begin{bmatrix} d\hat{i_1}/dt \\ d\hat{i_2}/dt \\ d\hat{i_3}/dt \\ d\hat{i_4}/dt \\ d\hat{v_c}/dt \end{bmatrix} = \begin{bmatrix} \mathrm{A_s} & \mathrm{A_1} & \mathrm{A_2} & \mathrm{A_1} & \frac{-(B_s+2B_1+B_2)R_{\text{load}}}{(R_{\text{load}}+R_{\text{esr}})} \\ \mathrm{A_1} & \mathrm{A_s} & \mathrm{A_1} & \mathrm{A_2} & \frac{-(B_s+2B_1+B_2)R_{\text{load}}}{(R_{\text{load}}+R_{\text{esr}})} \\ \mathrm{A_2} & \mathrm{A_1} & \mathrm{A_s} & \mathrm{A_1} & \frac{-(B_s+2B_1+B_2)R_{\text{load}}}{(R_{\text{load}}+R_{\text{esr}})} \\ \mathrm{A_1} & \mathrm{A_2} & \mathrm{A_1} & \mathrm{A_s} & \frac{-(B_s+2B_1+B_2)R_{\text{load}}}{(R_{\text{load}}+R_{\text{esr}})} \\ \frac{R_{\text{load}}}{(R_{\text{load}}+R_{\text{esr}})C} & \frac{R_{\text{load}}}{(R_{\text{load}}+R_{\text{esr}})C} & \frac{R_{\text{load}}}{(R_{\text{load}}+R_{\text{esr}})C} & \frac{R_{\text{load}}}{(R_{\text{load}}+R_{\text{esr}})C} & -\frac{1}{(R_{\text{load}}+R_{\text{esr}})C} \end{bmatrix} \begin{bmatrix} \hat{i_1} \\ \hat{i_2} \\ \hat{i_3} \\ \hat{i_4} \\ \hat{v_c} \end{bmatrix} + V_{\text{in}} \begin{bmatrix} B_s & B_1 & B_2 & B_1 \\ B_1 & B_s & B_1 & B_2 \\ B_2 & B_1 & B_s & B_1 \\ B_1 & B_2 & B_1 & B_s \\ 0 & 0 & 0 & 0 \end{bmatrix} \begin{bmatrix} \hat{d_1} \\ \hat{d_2} \\ \hat{d_3} \\ \hat{d_4} \end{bmatrix} \tag{18}$$

$$\begin{bmatrix} \frac{d\Sigma\hat{i_k}}{dt} \\ \frac{d\hat{v_c}}{dt} \end{bmatrix} = \underbrace{\begin{bmatrix} A_s + 2A_1 + A_2 & 4\frac{-(B_s+2B_1+B_2)R_{\text{load}}}{(R_{\text{load}}+R_{\text{esr}})} \\ \frac{R_{\text{load}}}{(R_{\text{load}}+R_{\text{esr}})C} & -\frac{1}{(R_{\text{load}}+R_{\text{esr}})C} \end{bmatrix}}_{\mathbf{A}} \begin{bmatrix} \Sigma\hat{i_k} \\ \hat{v_c} \end{bmatrix} + \underbrace{V_{\text{in}} \begin{bmatrix} B_s + 2B_1 + B_2 \\ 0 \end{bmatrix}}_{\mathbf{B}} \hat{d} \tag{19}$$

where v_o has the relation with v_c of (17) when the considering of the output capacitor esr,

$$\begin{cases} \hat{v_o} = \frac{R_{\text{load}}}{R_{\text{load}}+R_{esr}}\hat{v_c} + (R_{\text{load}} \,//\, R_{esr})\,\Sigma\hat{i_k} \\ \frac{d\hat{v_c}}{dt} = \frac{R_{\text{load}}}{(R_{\text{load}}+R_{\text{esr}})C}\Sigma\hat{i_k} - \frac{\hat{v_c}}{(R_{\text{load}}+R_{\text{esr}})C} \end{cases} \tag{17}$$

Dulplicate the procedure in (16) for each phase, and combining (17), the full equation in (4) can be transformed to the state space equation in (18). Where all the constants in the matrix are listed as (20)

$$\begin{aligned} \mathrm{A_s} &= -B_s R_{\text{wind}} - (R_{\text{load}} \,//\, R_{\text{esr}})\,(B_s + 2B_1 + B_2) \\ \mathrm{A_1} &= -B_1 R_{\text{wind}} - (R_{\text{load}} \,//\, R_{\text{esr}})\,(B_s + 2B_1 + B_2) \\ \mathrm{A_2} &= -B_2 R_{\text{wind}} - (R_{\text{load}} \,//\, R_{\text{esr}})\,(B_s + 2B_1 + B_2) \end{aligned} \tag{20}$$

Since the full state space equation is now obtained, a simplification can be used to find the uniform duty cycle perturbation dynamics on output voltage and total current, (18) can be downgrade to (19) when $d_1 = d_2 = d_3 = d_4 = d$.

The output state vector should be shortened accordingly,

$$\begin{bmatrix} \sum\hat{i_k} \\ \hat{v_o} \end{bmatrix} = \underbrace{\begin{bmatrix} 1 & 0 \\ \frac{R_{\text{load}}\,R_{\text{esr}}}{(R_{\text{load}}+R_{\text{esr}})} & \frac{R_{\text{load}}}{(R_{\text{load}}+R_{\text{esr}})} \end{bmatrix}}_{\mathbf{E}} \begin{bmatrix} \Sigma\hat{i_k} \\ \hat{v_c} \end{bmatrix} \hat{d} \tag{21}$$

Then the transfer function from duty cycle to output voltage and total output current can be calculated by the reduced order model as (22) and (23) respectively.

$$G_{d\to v_o} = \frac{\hat{v_o}}{\hat{d}} = \mathbf{E}_{row2}(s\mathbf{I} - \mathbf{A})^{-1}\mathbf{B} \tag{22}$$

$$G_{d\to \Sigma i_k} = \frac{\Sigma\hat{i_k}}{\hat{d}} = \mathbf{E}_{row1}(s\mathbf{I} - \mathbf{A})^{-1}\mathbf{B} \tag{23}$$

TABLE II
DESIGN PARAMETERS FOR THE DYNAMIC ANALYSIS

R_{wind}	R_{esr}	R_{load}	C	L_s	V_{in}
8 mΩ	0.9 mΩ	40 mΩ	200 μF	1420 nF	12 V

The theoretical bode plot in Fig. 5 is formulated by the parameters in Table II. Coherent to the analysis in the previous section, the positive coupling has no advantages in the buck converter design while negative coupling offers a wider bandwidth than non-coupled situations.

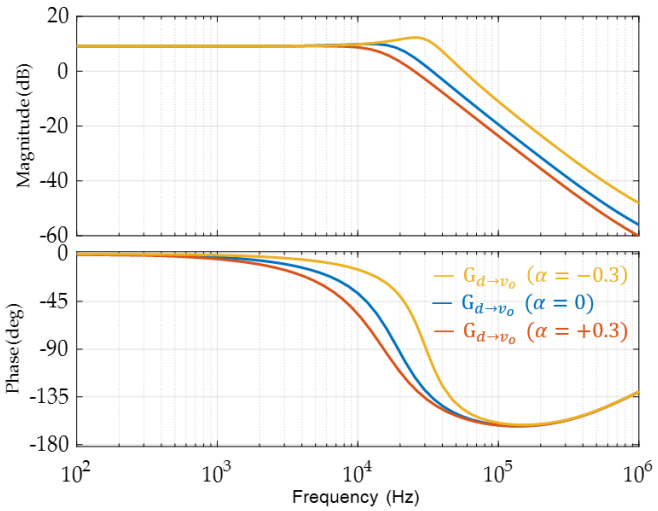

(a) Duty cycle change to output voltage dynamics

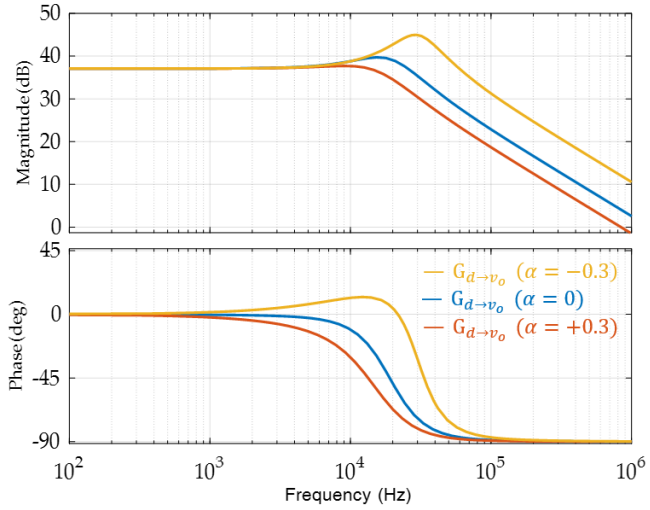

(b) Duty cycle change to output current dynamics

Fig. 5. Dynamics for the four-phase DCIAarry buck converter

III. Matrix-type coupling implementation and FEA simulation verification

Even though proposed coupling structure does not rely on the geometry of the magnetic components, but purely on the winding structure, special arrangements of magnetics may still enhance, or weaken the characteristic of coupling.

Fig. 6 is the PCB winding design for the proposed coupling structure, by connecting the head and tail of the inductors in a DCIArray, As shown in Fig. 7, a cross or circular matrix-type coupled inductor structure can be realized for high power density application.

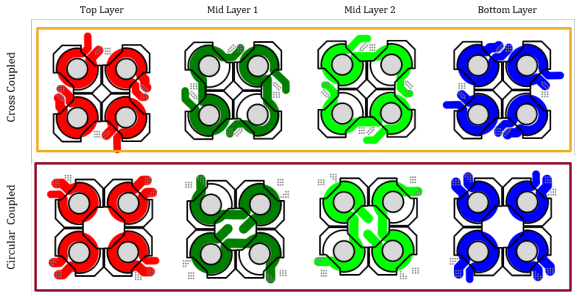

(a) Negative coupled in adjacent phases

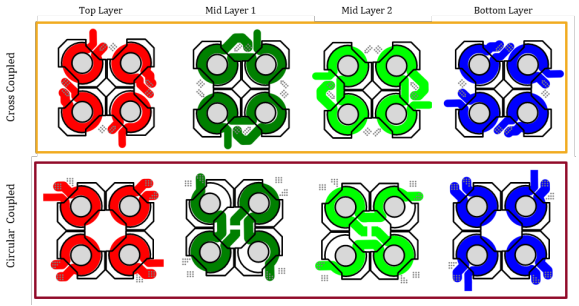

(b) Positive coupled in adjacent phases

Fig. 6. Circular and cross matrix-type coupled pcb winding structure

However, because of the spacial approximation of the magnetic components, the coupling behavior will differ from the analyitical model proposed in the section II. Apart from the adjacent phases coupling, there would also exist coupling between diagonal phases, the coupling manner will slightly diverge from pure independent inductors and be closer to matrix-coupled inductor in [16], [17], [18]. So we will discuss the influence of this magnetic integration on coupling and converter performance in the subsection.

A. matrix-type integration impact on coupling manner and phase current

If all phase inductors' center leg flux has the same direction, then there is only one feasible winding structure for adjacent phase to implement negative coupling, this is valid for both cross and circular structure. However, if the termination of current can be swapped, then positive adjacent coupling can be transformed to the negative, as depicted in Fig. 8.

The diagonal phases maintain their coupling coefficient after swapping, however the coupling coefficient of the adjacent

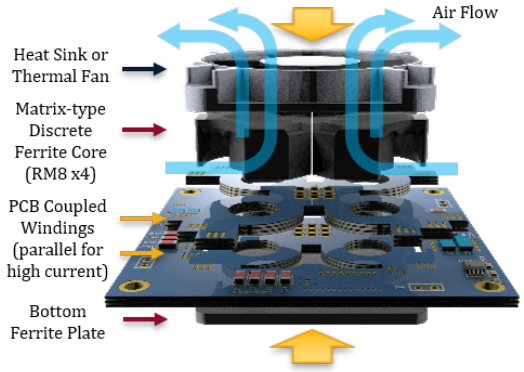

(a) matrix-type discrete coupled buck converter assembly

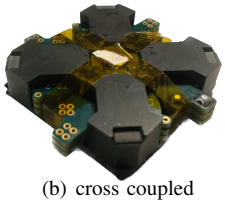

(b) cross coupled

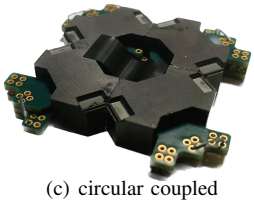

(c) circular coupled

Fig. 7. Hardware prototype and assembly schematic

TABLE III
FEA simulated inductance results for different matrix-type coupled structure

	symbol	cross neg	circular neg	cross pos	circular pos
Simulated	L_{s1} (nH)	1175	1407	1565	1260
	L_{s2} (nH)	1192	1388	1648	1248
	L_{s3} (nH)	1178	1401	1601	1263
	L_{s4} (nH)	1187	1385	1593	1247
	M_{12} (nH)	-390	-412	323	361
	M_{13} (nH)	14	105	-155	-30
	M_{14} (nH)	-394	-415	322	355
	M_{23} (nH)	-394	-416	338	356
	M_{24} (nH)	14	106	-156	-28
	M_{34} (nH)	-388	-412	334	362
	R_{wind} (3 parallel) (mΩ)	3.21	3.17	3.40	3.05
Modeled	L_s (nH)	1182	1182	1630	1182
	$M_{12}, M_{23}, M_{34}, M_{14}$	-407	-407	489	407
	M_{13}, M_{24} (nH)	0	0	0	0

phases will alter its sign. Now, there are two distinct routing methods for realizing negative coupled inductors for cross and circular structures, respectively.

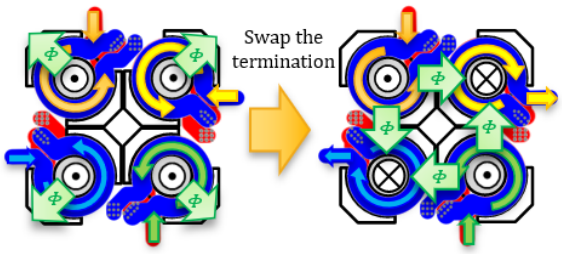

Fig. 8. Swapping the input termination of winding to alter the coupling structure

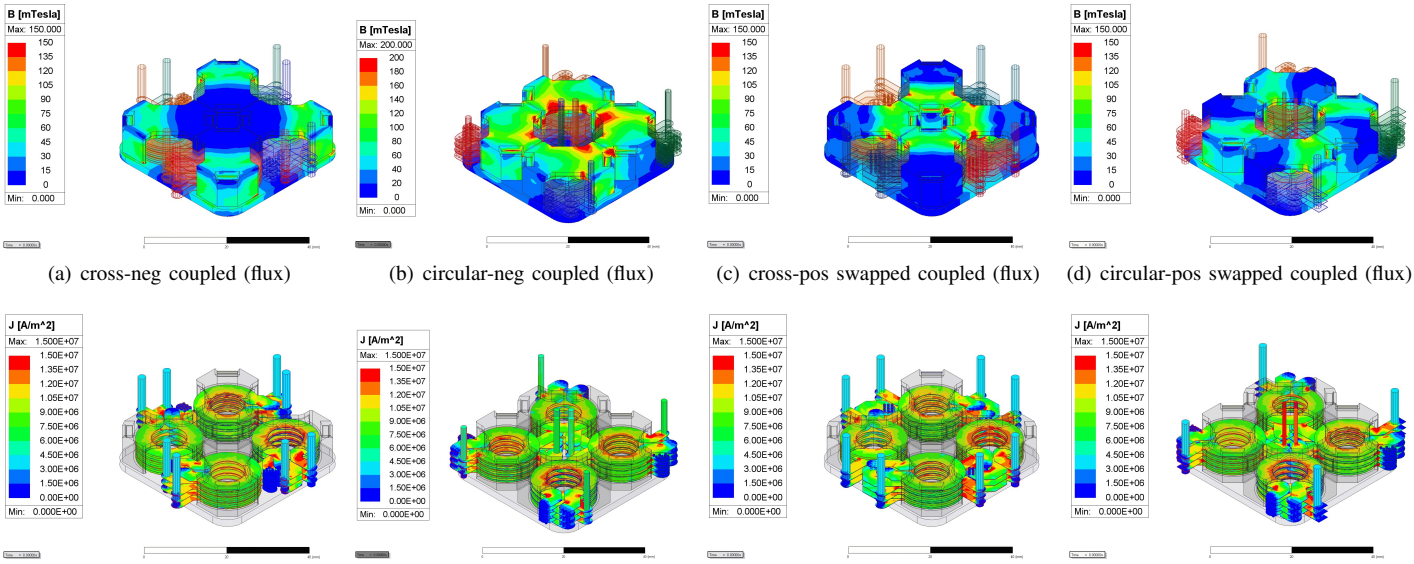

(a) cross-neg coupled (flux) (b) circular-neg coupled (flux) (c) cross-pos swapped coupled (flux) (d) circular-pos swapped coupled (flux)

(e) cross-neg coupled (current) (f) circular-neg coupled (current) (g) cross-pos swapped coupled (current) (h) circular-pos swapped (current)

Fig. 9. FEA transient simulation results of flux and current distribution for all matrix-type negative coupled inductor

The inductance differences of the proposed four-structure are calculated using a finite element analysis program (ANSYS Maxwell). The simulated values and matching theoretical modeling values were presented in Table III. The matrix core is made up of four RM8 ferrite cores, a ferrite plat is attached as magnetic cover in each case with a 0.5mm gap. To reduce the inductor's direct current resistance, three 4-layer PCB windings of the same design are stacked up for paralleling.

Simulation results suggests that both cross and circular structure suffered from the matrix integration. In most cases, the coupling coefficient will be lower, but in cases of main flux and mutual flux share the same reluctance, that is, when windings are cross negative coupled, the coupling will be strengthened. The diagnal coupling is severe in case of cross positive coupled windings. However, all these distortion may not impact the phase current seriously as simulated in Fig. 10, even if the diagonal coupling is taken into consideration, the main difference is the current slope during the coupling intervals.

B. matrix-type integration impact on flux/current distribution

According to the finite element transient simulation in Fig. 9, the circular-positive swapped structure and cross-negative coupled structure have the better flux distribution among the four distinct coupling structures. In the cross-positive swapped structure, all phases' flux will concentrate on the center leg, making the side legs of magnetics unnecessary, which is undesirable for the design. While the circular-negative structure, suffered from same direction output current, will accumulate high density of circulating flux on the upper surface of inductors, may also deteriorate the thermal performance.

Overall, the current distribution in all four cases are similar, so the most loss difference will comes from the magnetic components. Therefore, the recommended coupling structure for matrix-type DCIArray is cross-negative coupled structure and circular positive swapped structure.

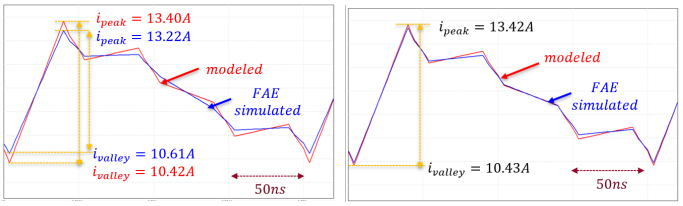

(a) circular-negative coupled (b) cross-positive swapped coupled

Fig. 10. Comparison of Matrix-type coupling with theoretical model

IV. Experiment Verification and Conclusion

Finally, a prototype for the proposed adjacent phase coupling structure was built, and experiment are implemented with both negative and positive coupled. The phase current waveform are basically coherent with the analytical model in the lecture. As shown in the Fig. 11.

TABLE IV
MEASURED INDUCTANCE VALUE FOR THE PROPOSED COUPLED INDUCTOR

symbol	cross neg	circular pos
L_{s1} (nH)	1404	1216
L_{s2} (nH)	1364	1232
L_{s3} (nH)	1356	1196
L_{s4} (nH)	1352	1236
M_{12} (nH)	-507	246
M_{13} (nH)	115	-124
M_{14} (nH)	-459	273
M_{23} (nH)	-502	243
M_{24} (nH)	104	-128
M_{34} (nH)	-467	268
R_{wind} (3 parallel) (mΩ)	8.97	6.48

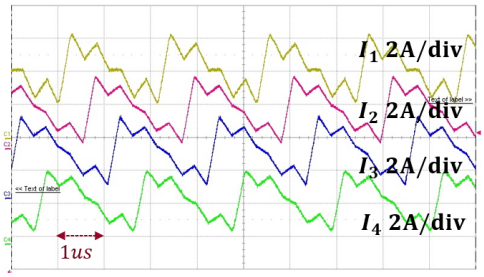

(a) Proposed negative coupled

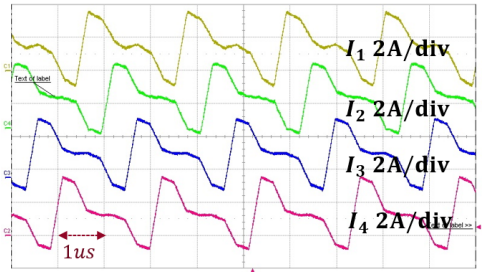

(b) Proposed positive coupled

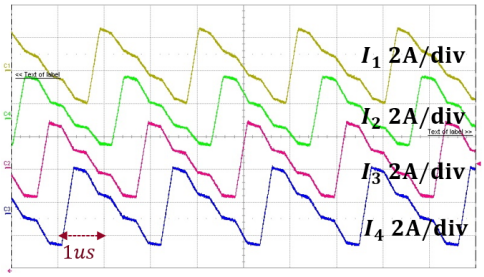

(c) Commercial available CL1108-4 [19]

Fig. 11. Experiment waveform of proposed coupled structure

The measure coupled inductor parameters are listed in table IV and are quite similar to the values predicted by the FAE, supporting the validity of the analysis that was introduced in the paper. For comparison purpose, a commercial available coupled inductor CL1108-4 [19] is also tested with same configuration, the current waveform indicates that the coupling structure in the inductor is a even positive for all phases, which is not preferable for the high transient response uses.

In conclusion, this paper proposed a generalized multiphase symmetrical coupled inductor structure, which is suitable for either discrete coupled inductor structure and matrix-type integration. The coupling coefficient adjustment is easy to implement without the requirement of customized ferrite cores compared to conventional designs. The coupling between adjacent phase maintain the benefits of high steady-state inductor and low transient state inductance compared to full symmetrical structure. And the matrix-type integration may improve the flux distribution without introducing much distortion to the coupling behavior.

REFERENCES

1 Li, J., Stratakos, A., Schultz, A., and Sullivan, C., "Using coupled inductors to enhance transient performance of multi-phase buck converters," in *Nineteenth Annual IEEE Applied Power Electronics Conference and Exposition, 2004. APEC '04.*, vol. 2, Feb. 2004, pp. 1289–1293 vol.2.

2 Zhu, G., McDonald, B. A., and Wang, K., "Modeling and Analysis of Coupled Inductors in Power Converters," *IEEE Transactions on Power Electronics*, vol. 26, no. 5, pp. 1355–1363, May 2011.

3 Lu, Z. and Chen, W., "Multi-Phase Inductor Coupling Scheme with Balancing Winding in VRM Applications," in *APEC 07 - Twenty-Second Annual IEEE Applied Power Electronics Conference and Exposition*, Feb. 2007, pp. 731–735.

4 Zhu, F. and Li, Q., "Coupled Inductors With an Adaptive Coupling Coefficient for Multiphase Voltage Regulators," *IEEE Transactions on Power Electronics*, vol. 38, no. 1, pp. 739–749, Jan. 2023.

5 Zhou, D. H., Elasser, Y., Baek, J., and Chen, M., "Reluctance-Based Dynamic Models for Multiphase Coupled Inductor Buck Converters," *IEEE Transactions on Power Electronics*, vol. 37, no. 2, pp. 1334–1351, 2022.

6 Baek, J., Elasser, Y., Radhakrishnan, K., Gan, H., Douglas, J. P., Krishnamurthy, H. K., Li, X., Jiang, S., Sullivan, C. R., and Chen, M., "Vertical Stacked LEGO-PoL CPU Voltage Regulator," *IEEE Transactions on Power Electronics*, vol. 37, no. 6, pp. 6305–6322, Jun. 2022.

7 Wang, P., Zhou, D. H., Elasser, Y., Baek, J., and Chen, M., "Matrix Coupled All-in-One Magnetics for PWM Power Conversion," *IEEE Transactions on Power Electronics*, vol. 37, no. 12, pp. 15 035–15 050, 2022.

8 Elasser, Y., Baek, J., Sullivan, C. R., and Chen, M., "Modeling and Design of Vertical Multiphase Coupled Inductors with Inductance Dual Model," in *2021 IEEE Applied Power Electronics Conference and Exposition (APEC)*, Jun. 2021, pp. 1717–1724.

9 Chen, M. and Sullivan, C. R., "Unified Models for Coupled Inductors Applied to Multiphase PWM Converters," *IEEE Transactions on Power Electronics*, vol. 36, no. 12, pp. 14 155–14 174, 2021.

10 Yang, Y., Liu, Z., Lee, F. C., and Li, Q., "Multi-phase coupled and integrated inductors for critical conduction mode totem-pole PFC converter," in *2017 IEEE Applied Power Electronics Conference and Exposition (APEC)*, Mar. 2017, pp. 1804–1809.

11 Yang, Y., Guan, T., Zhang, S., Jiang, W., and Huang, W., "More Symmetric Four-Phase Inverse Coupled Inductor for Low Current Ripples & High-Efficiency Interleaved Bidirectional Buck/Boost Converter," *IEEE Transactions on Power Electronics*, vol. 33, no. 3, pp. 1952–1966, Mar. 2018.

12 Mayer, R., Kattel, M. B. E., and Oliveira, S. V. G., "Multiphase Interleaved Bidirectional DC/DC Converter With Coupled Inductor for Electrified-Vehicle Applications," *IEEE Transactions on Power Electronics*, vol. 36, no. 3, pp. 2533–2547, Mar. 2021.

13 Wong, P.-L., Xu, P., Yang, P., and Lee, F., "Performance improvements of interleaving VRMs with coupling inductors," *IEEE Transactions on Power Electronics*, vol. 16, no. 4, pp. 499–507, Jul. 2001.

14 Yang, Y., Mu, M., Liu, Z., Lee, F. C., and Li, Q., "Common mode EMI reduction technique for interleaved MHz critical mode PFC converter with coupled inductor," in *2015 IEEE Energy Conversion Congress and Exposition (ECCE)*, Sep. 2015, pp. 233–239.

15 Yang, F., Ruan, X., Yang, Y., and Ye, Z., "Interleaved Critical Current Mode Boost PFC Converter With Coupled Inductor," *IEEE Transactions on Power Electronics*, vol. 26, no. 9, pp. 2404–2413, Sep. 2011.

16 Li, M., Liu, Y., Ouyang, Z., and Andersen, M. A. E., "Butterfly Interleaving Winding Arrangements for Multiphase Coupled Inductors," *IEEE Transactions on Power Electronics*, pp. 1–13, 2022.

17 Lyu, Y., Sanusi, B. N., and Ouyang, Z., "Modeling and Analysis of Coupling Effect in Four Legged Core for Multi-phase Buck Converter," in *2023 IEEE Applied Power Electronics Conference and Exposition (APEC)*, Mar. 2023, pp. 3307–3313.

18 Zhou, D., Elasser, Y., Baek, J., Sullivan, C. R., and Chen, M., "Inductance Dual Model and Control of Multiphase Coupled Inductor Buck Converter," in *2020 IEEE 21st Workshop on Control and Modeling for Power Electronics (COMPEL)*, Nov. 2020, pp. 1–8.

19 "CL1108-4-50TR-R — Eaton CL1108 inductor," https://www.eaton.com/us/en-us/skuPage.CL1108-4-50TR-R.html.